Electronic Supplementary Information

A cost-effective Ca-doped Li_2ZrCl_6 halide solid electrolyte for all-solid-state lithium batteries

Xingkun Liu, Fanghui Mi and Chunwen Sun*

School of Chemical & Environmental Engineering, China University of Mining and Technology-Beijing, Beijing 100083, P. R. China.

*Email: csun@cumtb.edu.cn (C. Sun)

Experimental section

Materials synthesis

The halide solid electrolytes $Li_{2+x}Zr_{1-x}Ca_xCl_6$ ($0.0 \leq x \leq 0.2$) were synthesized through a facile mechanochemical milling route. The stoichiometric amounts of the initial materials of LiCl (99%, Macklin), $ZrCl_4$ (98%, Macklin), $CaCl_2$ (99.99%, Macklin) were firstly mixed manually for 10 min in an agate mortar with a ball-to-powder mass ratio of 25:1. Then the mixture was further milled in zirconia pots (50 ml) using zirconia balls of Φ= 10, 8 and 5 mm with a weight ratio of 2 : 3 : 5 in a planetary mill (YXQM-2L, MITR) at 600 rpm for 28 h (6min of milling, followed by 2 min of rest). The pots were opened, and the precursors were ground several times to ensure homogenization of the powder during the milling process. The zirconia jars were tightly sealed with fluor rubber sealing rings to yield the final products. All operations, such as weighting, sealing, collecting and storing, were conducted in an Ar-filled glove box.

Materials characterizations

X-ray diffraction measurements were performed using a PANalytical Empyrean diffractometer with Cu Ka radiation (l = 1.5418 Å), and the powder samples were sealed in a sample holder under an Ar atmosphere with Kapton film to avoid air exposure. Rietveld refinement was performed using GSAS II.[1,2] In addition, the XRD patterns were obtained to be used for Rietveld refinement at scan rate of 2 degrees per minute, while others were collected at 7.5 degrees per minute.

X-ray photoelectron spectroscopy (XPS) data was collected by operating an ESCALAB 250Xi spectrometer (Thermo Fisher Scientific) with Al Kα achromatic X-rays.

BVSE calculations

BVSE calculations were based on corresponding structural models obtained from Rietveld refinement by the softBV program.[3,4] The different Li sites energies for the corresponding crystal structure were calculated against a 3D grid of points with 0.1 Å resolution by the transferable Morse-type softBV force field. The regions of low

BVSE indicate the preferred Li^+ ion migration pathways. All optimized structures based on three different channels are visualized using the VESTA software.[5]

Conductivity and activation energy measurements

The Li^+ conductivity of all as-milled halide SEs was obtained by cold-pressed method. The 60 mg of SE powder was placed between two stainless steel rods and pressed into a 10 mm diameter pellet in a home-made polyethererherketone (PEEK) mold at 2 tons for 1 min. Nyquist plots were recorded at a frequency from 1 MHz to 1 Hz using a Zennium electrochemical workstation to determine the temperature dependence of Li^+ conductivities from 30°C to 70°C. The activation energies (E_a) were further calculated using the equation: $\sigma T = \sigma_0 \exp(-E_a/k_B T)$, where σ is ionic conductivity, σ_0 is the prefactor, T is absolute temperature and k_B is the Boltzmann constant.[6]

The electronic conductivities of SEs were measured according to the direct current (DC) polarization curve using stainless steel sheet as ion blocking electrodes. The external applied voltage (1V) was adopted for 1 h ensuring the resultant current stabilized. The mold assembly process is the same as the described above.

Electrochemical measurements

Electrochemical stable window (ESW) of halide solid electrolytes were evaluated via linear sweep voltammetry (LSV) methods. 60 mg of as-milled halide SEs powder was firstly pressed in a PEEK mold of 10 mm diameter at 1.5 tons for 1 min. The working electrode was prepared by manually mixing SEs with vapor-grown carbon fibers (VGCFs) (Dongguan Kelude Innovation Technology, 99%) at mass ratio of 7:3. Then 20 mg of mixtures were uniformly dispersed on one side of SE pellet and pressed at 2 tons for 5 mins. 40 mg of LPSCl powder (Shenzhen Kejing Star Technology, 99%) was pressed at 1.5 tons for 5 mins on the other side of SE pellet. Finally, a thin Li foil (100 μm thickness, 10 mm diameter) was attached to be as the counter electrode. The LSV measurements were performed by a CHI604E electrochemical workstation on an asymmetric Li | LiPSCl-halide SE | halide SE + VGCF cell at a scan rate of 0.2 mV s^{-1}. All operations were conducted in an Ar-filled glove box (Vigor; O_2 below 1 ppm, H_2O below 1 ppm).

The ASSBs with different as-milled halide SEs were assembled in an Ar-filled glove box. The positive electrode was composed of the cathode materials (LCO or scNCM811, provided by Dongguan Kelude Innovation Technology) and halide SEs with a weight ratio of 7:3 via manually mixing for 30 mins. First of all, 55 mg of halide SEs powder was pressed under 1.5 tons for 2 mins in PEEK mold of 10 mm diameter. Then ~5 mg of cathode composite powder was evenly dispersed on one side of halide SEs pellet and pressed at 2 tons for 2 mins. 45 mg of LPSCl powder (Shenzhen Kejing Star Technology, 99%) was used as stable interlayer between halide SEs and anode and uniformly spread over another side of the Halide SEs pellet at 2 tons for 10 mins. Finally, a thin In foil (100 μm thickness, 10 mm diameter) was attached to the surface of LPSCl layer and a piece of Li foil (100 μm thickness, 6 mm diameter) was subsequently attached to the In foil. The ASSBs were further cycled under an external pressure of 100 Mpa employing a LAND CT2001A battery testing system.

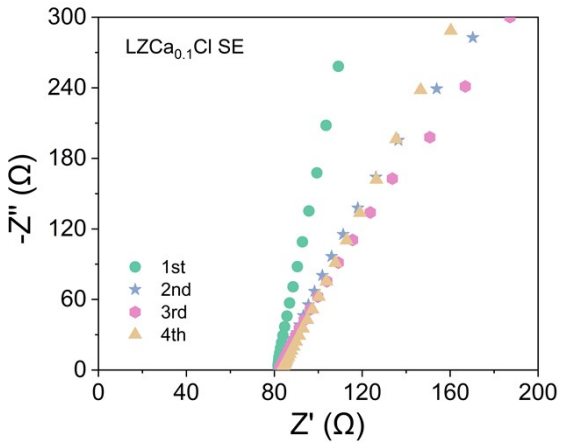

Fig. S1 The reproducibility of synthesis method for $LZCa_{0.1}Cl$.

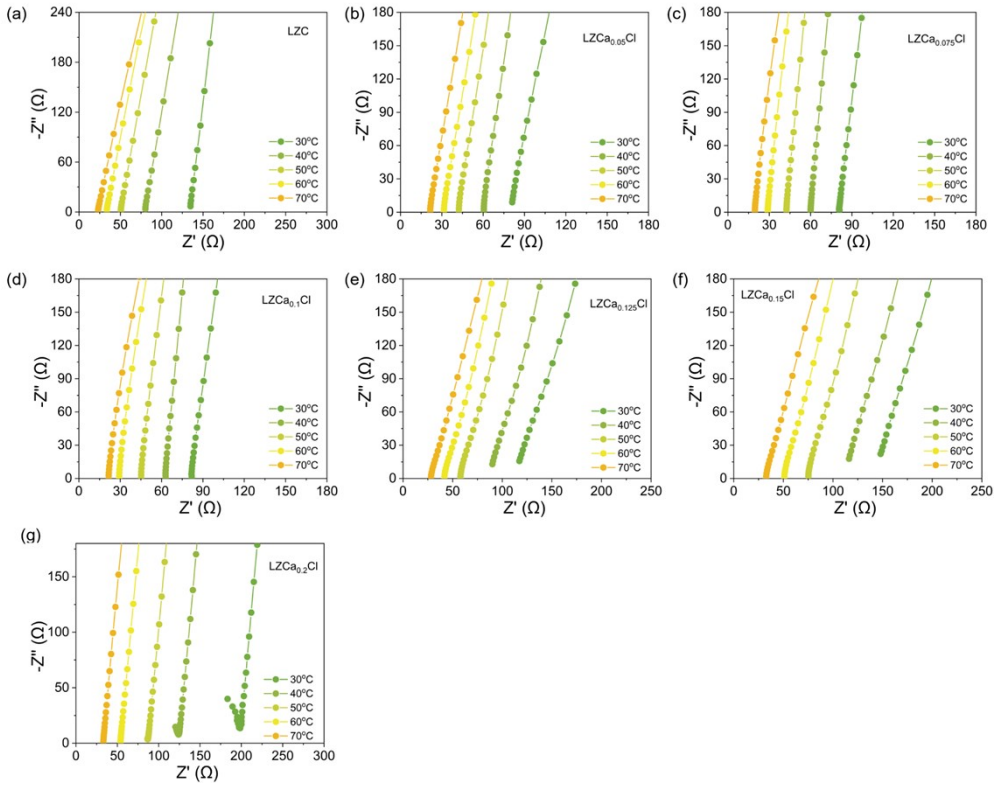

Fig. S2 Nyquist plots at different temperatures from 30°C to 70°C for $Li_{2+x}Zr_{1-x}Ca_xCl_6$ ($0.0 \leq x \leq 0.2$).

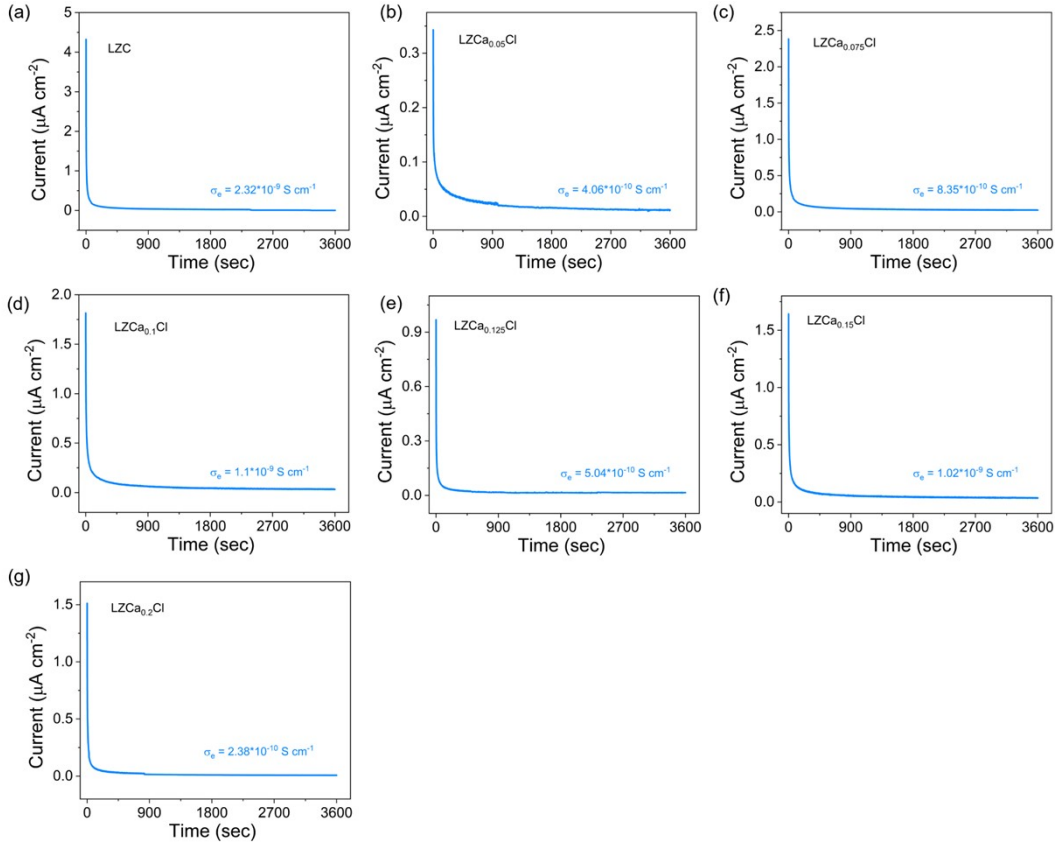

Fig. S3 The transient current behavior under DC bias for the $Li_{2+x}Zr_{1-x}Ca_xCl_6$ SEs with x = 0 (a), 0.05 (b), 0.075 (c), 0.1 (d), 0.125 (e), 0.15 (f) and 0.2 (g) with stainless steel electrodes at RT.

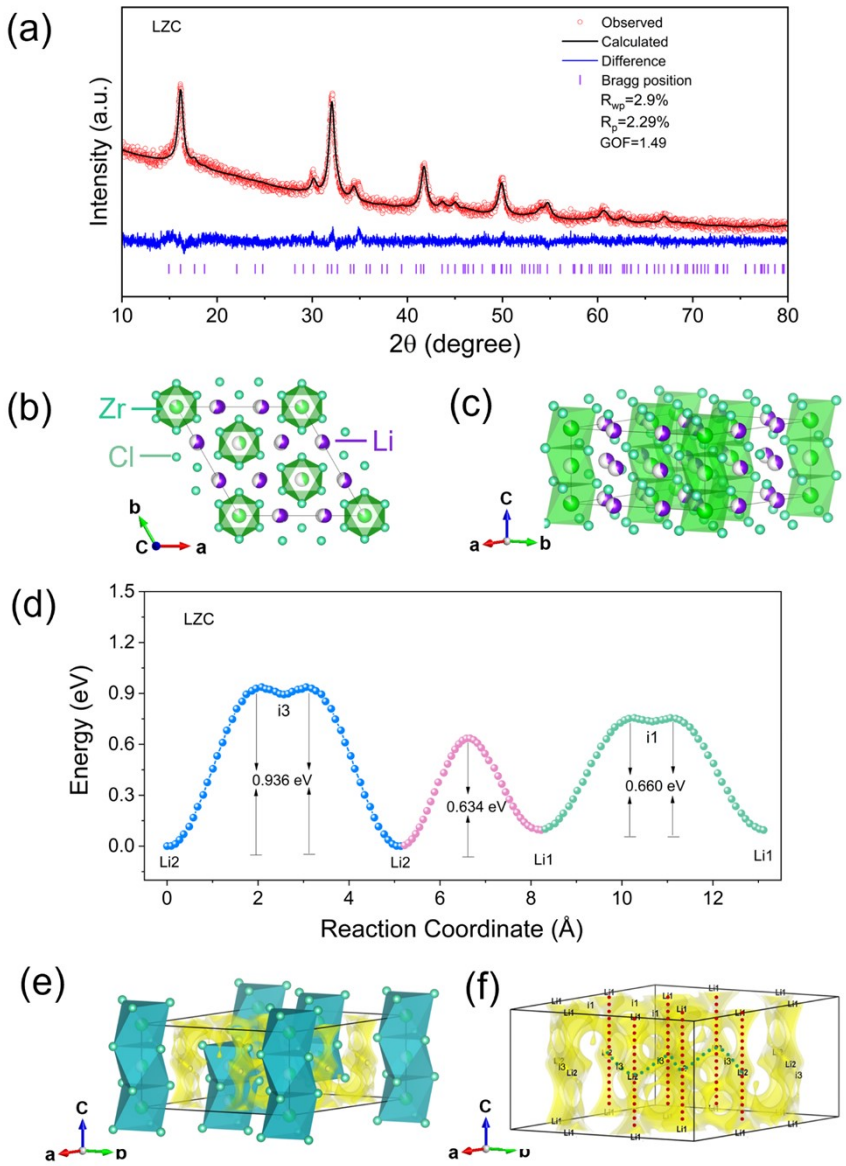

Fig. S4 (a) Rietveld refinement of XRD pattern for LZC at RT. (b, c) The crystal structure of LZC derived from Rietveld refinement. (d) Energy profiles of the migration pathways in LZC. (e) The crystal structure of LZC with Li^+ potential map. (f) Li^+ migration pathway of LZC.

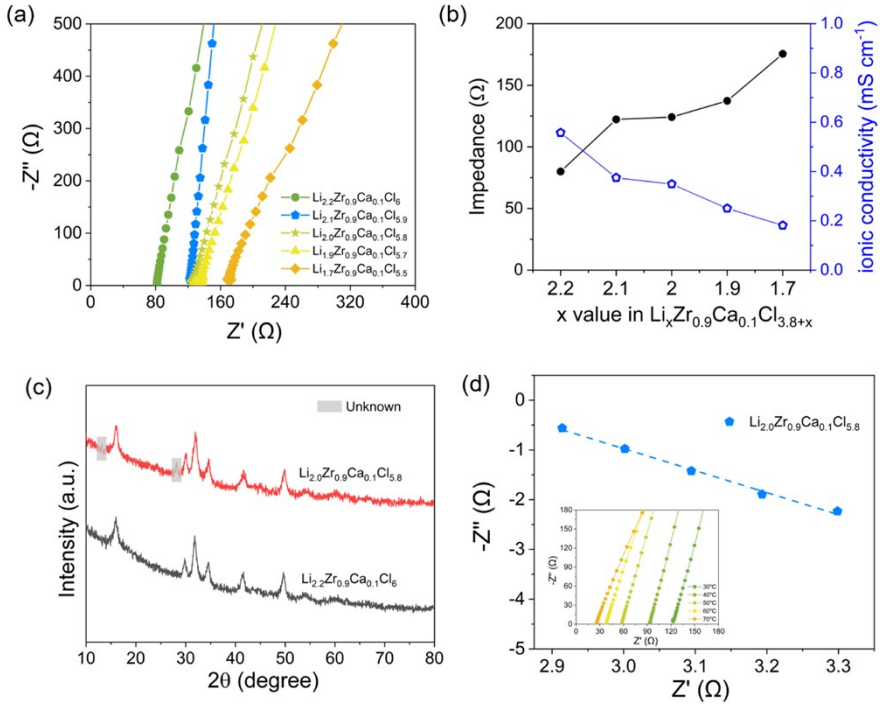

Fig. S5 (a) Nyquist plots of $Li_xZr_{0.9}Ca_{0.1}Cl_{3.8+x}$ ($1.7 \leq x \leq 2.2$) SEs at 30°C at RT. (b) Ionic conductivity and impedance for $Li_xZr_{0.9}Ca_{0.1}Cl_{3.8+x}$ ($1.7 \leq x \leq 2.2$) SEs. (c) XRD patterns of $Li_{2.2}Zr_{0.9}Ca_{0.1}Cl_6$ and $Li_{2.0}Zr_{0.9}Ca_{0.1}Cl_{5.8}$ at RT. (d) Arrhenius plot of $Li_{2.0}Zr_{0.9}Ca_{0.1}Cl_{5.8}$ with Nyquist plots at different temperatures from 30°C to 70°C for $Li_{2.0}Zr_{0.9}Ca_{0.1}Cl_{5.8}$.

As shown in Fig. S4 a-b, as the contents of Li^+ carriers reduce from 2.2 to 1.7, the impedance gradually increases from 80.1 to 175.8 Ω, showing that the increase of Li^+ carriers is beneficial for enhancing Li^+ conductivity. The $Li_{2.0}Zr_{0.9}Ca_{0.1}Cl_{5.8}$ which is the same Li^+ carriers with Li_2ZrCl_6 were chosen to be further explored. It is noteworthy that the ionic conductivity of $Li_{2.0}Zr_{0.9}Ca_{0.1}Cl_{5.8}$ (0.36 mS cm^{-1}) still is higher than that of LZC (0.29 mS cm^{-1}), which is strongly related with Ca doping in LZC. The XRD pattern of $Li_{2.0}Zr_{0.9}Ca_{0.1}Cl_{5.8}$ was measured, peak locations of which mostly match with $Li_{2.2}Zr_{0.9}Ca_{0.1}Cl_6$ in Fig. S4c. However, two unknown characteristic peaks were observed at about 14° and 28°. The Nyquist plot of $Li_{2.0}Zr_{0.9}Ca_{0.1}Cl_{5.8}$ was obtained within the range of 30°C-70°C and Arrhenius plot of that was calculated with activation energy of 0.38 eV in Fig. S4d.

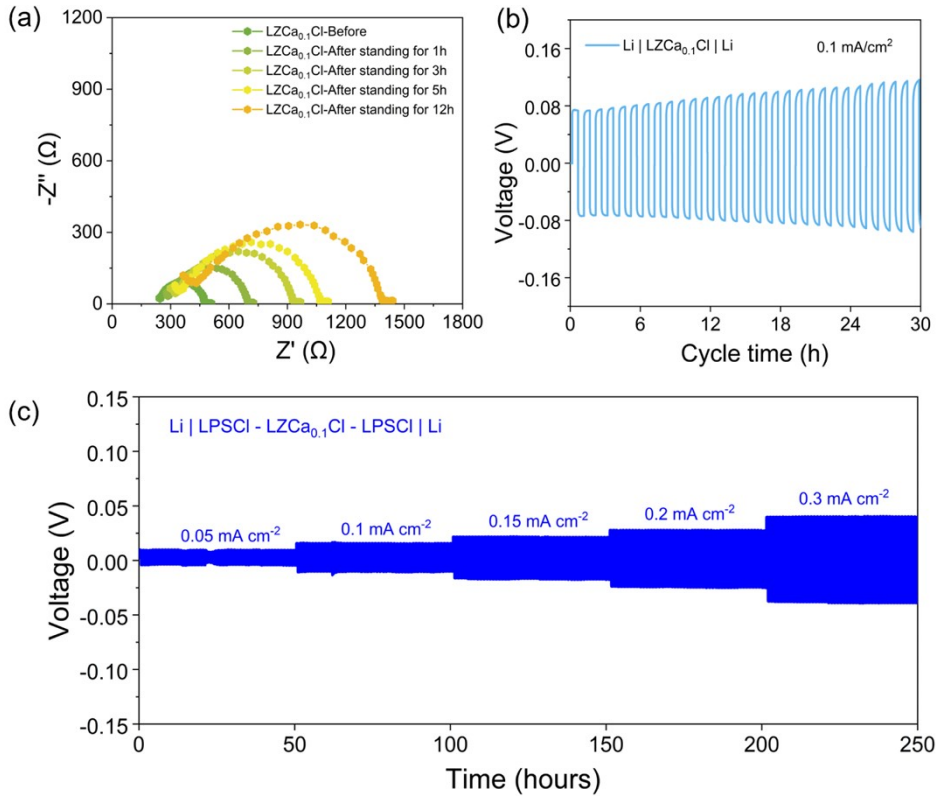

Fig. S6 (a) Nyquist plots of the symmetric Li |$LZCa_{0.1}Cl$| Li cell with different standing time at RT. (b) Voltage profile for Li |$LZCa_{0.1}Cl$| Li cell at a current density of 0.1mA cm^{-2}. (c) Voltage profile of Li | LPSCl-$LZCa_{0.1}Cl$-LPSCl | Li cell with different current densities from 0.05 to 0.3 mA cm^{-2}.

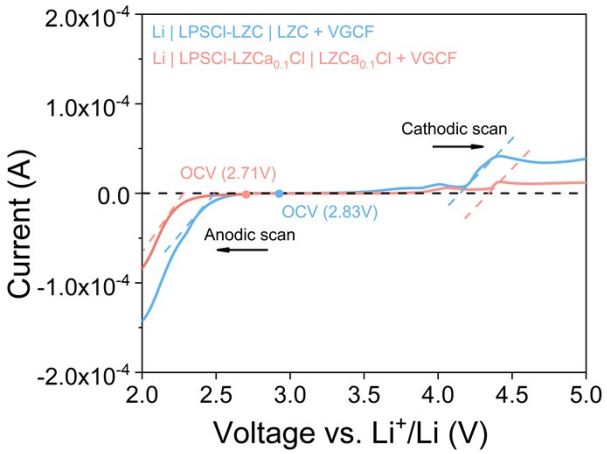

Fig. S7 LSV curves to reflect stable electrochemical window of LZC and $LZCa_{0.1}Cl$ at a scan rate of 0.2 mV s^{-1}.

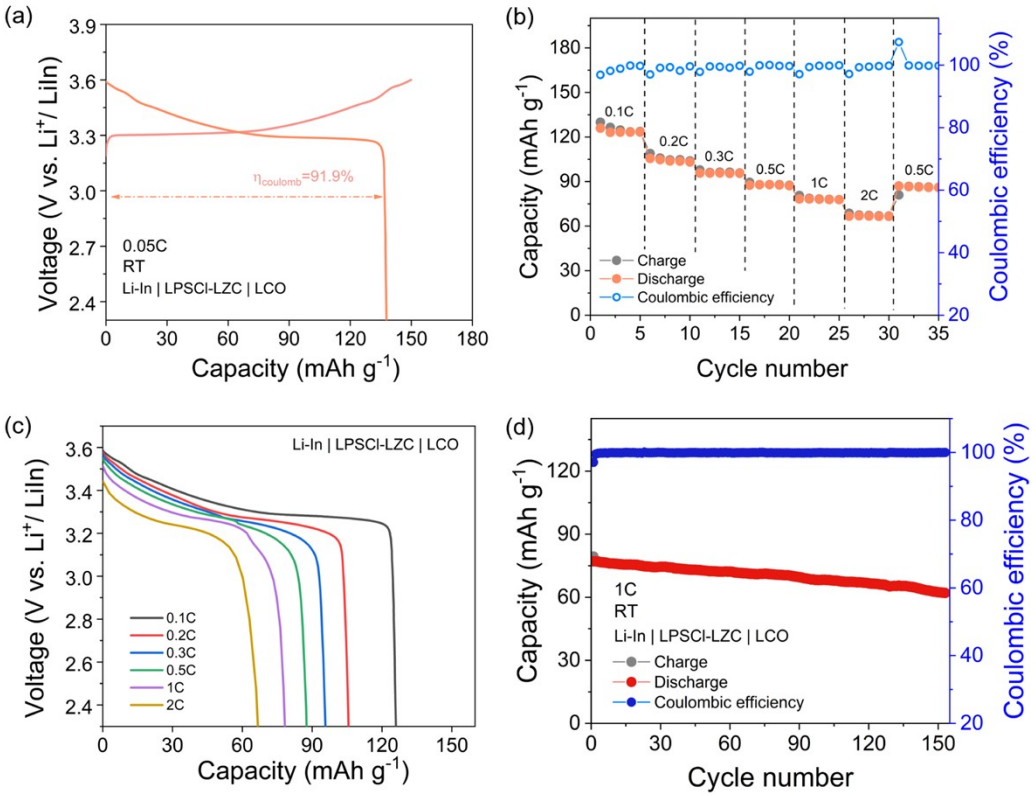

Fig. S8 Electrochemical performance of Li-In | LPSCl-LZC | LCO cell. (a) Initial charge and discharge curves at 0.05C. (b) Rate capability at 0.1, 0.2, 0.3, 0.5, 1, 2C. (c) Discharge curves at 0.1, 0.2, 0.3, 0.5, 1, 2C. (d) Long-term cycling performance at 1C.

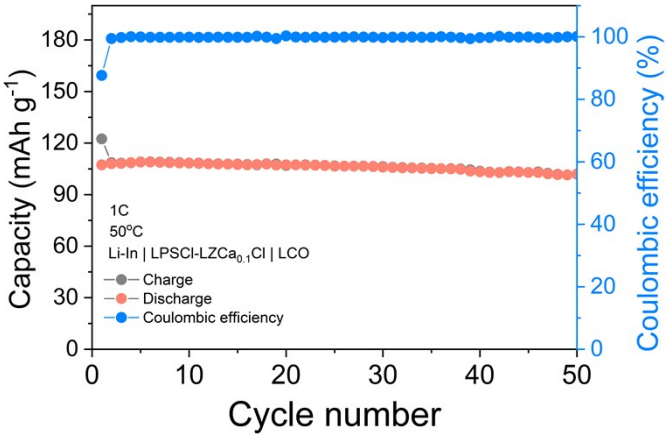

Fig. S9 Cycling performance at 1C under 50°C for Li-In | LPSCl-LZC$a_{0.1}$Cl | LCO cell.

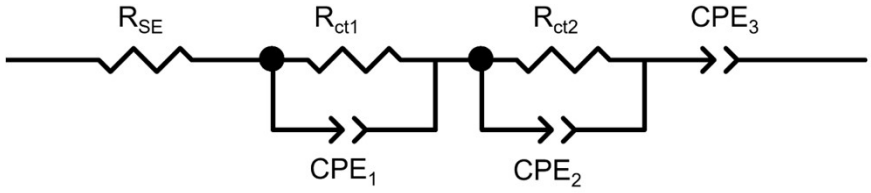

Fig. S10 The equivalent circuit employed to fit the EIS plots of ASSBs with the LZC and $LZCa_{0.1}Cl$ electrolytes.

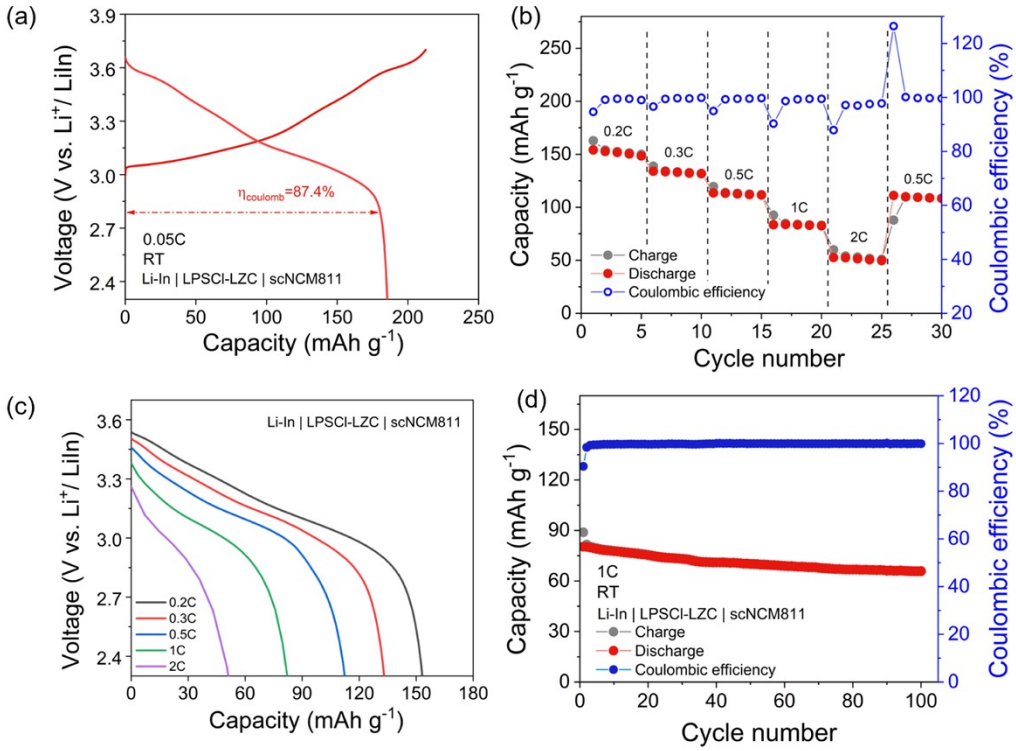

Fig. S11 Electrochemical performance of the Li-In | LPSCl-LZC | scNCM811 cell. (a) Initial charge and discharge curves at 0.05C. (b) Rate capability at 0.2, 0.3, 0.5, 1, 2C. (c) Discharge curves at 0.2, 0.3, 0.5, 1, 2C. (d) Long-term cycling performance at 1C.

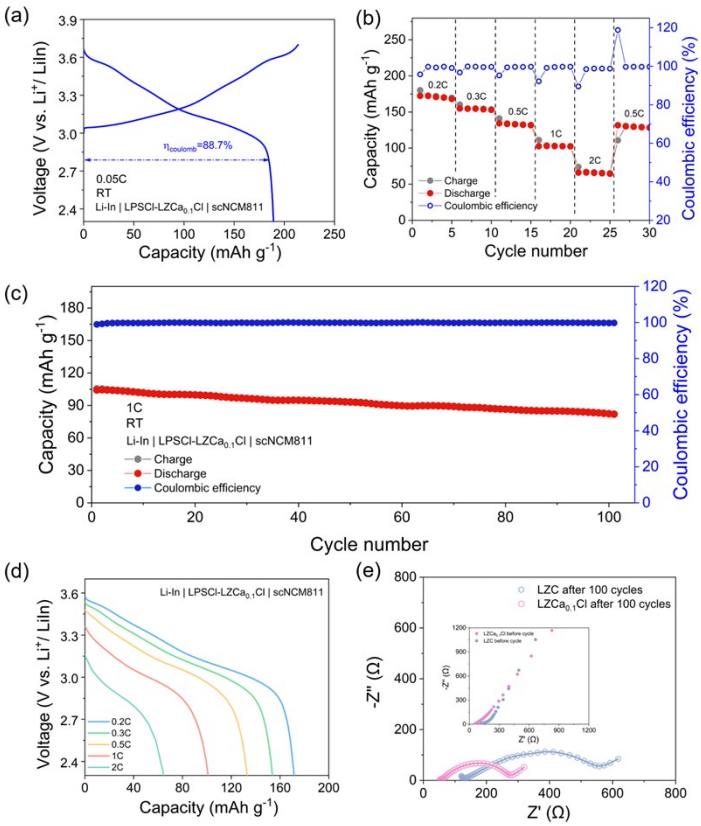

Fig. S12 Electrochemical performance of Li-In | LPSCl-$LZCa_{0.1}Cl$ | scNCM811 cell. (a) Initial charge and discharge curves at 0.05C. (b) Rate capability at 0.2C, 0.3C, 0.5C, 1C, 2C. (c) Cycling performance at 1C. (d) Discharge curves at 0.2C, 0.3C, 0.5C, 1C, 2C. (e) Nyquist plots for ASSBs with LZC and $LZCa_{0.1}Cl$ electrolytes before cycling and after 100 cycles.

ASSBs with scNCM811 cathode were evaluated between 2.3 and 3.7 V *vs.* Li-In/Li^+ at RT. The cell with $LZCa_{0.1}Cl$ exhibits a slightly higher discharge capacity of 189.7 mAh g^{-1} and initial Coulombic efficiency of 88.7% than those of LZC (185.9 mAh g^{-1} and 87.4%) at 0.05C (Fig. S9a and Fig. S10a). Likewise, compared to the cell with LZC electrolyte in Fig. S9b-c, the $LZCa_{0.1}Cl$-based cell shows a better rate performance, as shown in Fig. S10b and d. The average discharge capacities of the $LZCa_{0.1}Cl$ based cell are 170.7, 154.2, 133.0, 102.6 and 65.5 mAh g^{-1} at 0.2, 0.3, 0.5, 1 and 2C respectively, while those for LZC are only 152.3, 133.0, 112.6, 83.3 and 51.4 mAh g^{-1} at 0.2, 0.3, 0.5, 1 and 2C, respectively. Fig. S10c shows that the $LZCa_{0.1}Cl$-based cell demonstrates good cycling performance with a discharge capacity of 84.3 mAh

g^{-1} after 100 cycles at 1C, while the discharge capacity of the ASSB with LZC only maintains 65.8 mAh g^{-1} at 1C after 100 cycles (Fig.S9d). In addition to the high ionic conductivity compared to LZC, the superior comprehensive electrochemical performances for $LZCa_{0.1}Cl$-based cell might be related to the stable interfacial resistance. Thus, EIS measurements after 100 cycles were conducted and Nyquist plots were further fitted with the equivalent circuit in Fig. 4f. Apparently, the R_{ct2} of $LZCa_{0.1}Cl$-based cell (212 Ω) is less than half of that of LZC (469 Ω) in Table S5, indicating that Ca^{2+} substitution with a wider ESW is beneficial for stabilizing interface to achieve high discharge capacity and good rate capability.

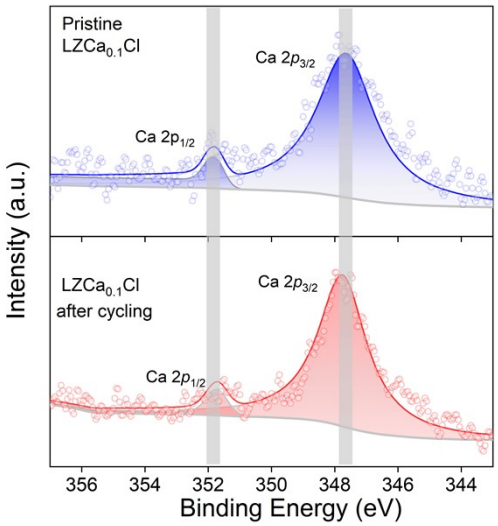

Fig. S13 XPS spectra of the pristine $LZCa_{0.1}Cl$ and LCO-$LZCa_{0.1}Cl$ cathode after 150 cycles for Ca 2p.

Table S1. Comparison of abundance of different elements in earth's crust and the prices of anhydrous raw materials for Zr-based halide electrolytes. Unit prices (CNY/mol) of different raw materials were estimated by laboratory-scale prices. All the prices listed here are obtained from Tansoole China office website except for MgCl2 from Macklin China office website. The abundance of elements in the earth's crust was referenced from Ref. 7.

Element	Abundance ppm	Chemical Formula	Product Description	Stock No. and Specification	Price, CNY	Unit price, CNY/kg	Unit price, CNY/mol
Li	20	LiCl	99%	016271086-20kg	5445	272.25	11.54
Zr	165	$ZrCl_4$	98%	013465274-25kg	8584.2	343.368	80.02
Ta	2	$TaCl_5$	99.9%	011517755-100g	1102	11020	3947.51
Ca	41500	$CaCl_2$	>97%	01585501-1kg	38	38	4.22
Mg	23300	$MgCl_2$	98%	M434107-5kg	270	54	5.14
Fe	56300	$FeCl_3$	99%	013474136-25kg	1331.9	53.276	8.64

As shown in Table S1, the abundance of Ca in earth's crust reaches up to 41500 ppm, which is much larger than those of Zr (165 ppm) and Ta (2 ppm). In addition, the abundance of Mg and Fe which were reported to be substitutional elements for LZC are respectively 23000 and 56300 ppm. Furthermore, unit prices (CNY/kg) of the corresponding different halide electrolytes (Li_2ZrCl_6, $Li_{2.1}Zr_{0.63}Ta_{0.27}Cl_6$, $Li_{2.2}Zr_{0.9}Ca_{0.1}Cl_6$, $Li_{2.1}Zr_{0.95}Mg_{0.05}Cl_6$ and $Li_{2.1}Zr_{0.9}Fe_{0.1}Cl_6$) are further calculated on the basis of the above raw materials' prices.[8-10] However, the price of LZC with rare metal Ta^{5+} doping inevitably reaches up to 3435.22 CNY/kg. Compared to LZC (324.41 CNY/kg), the Ca^{2+}-substituted LZC (311.47 CNY/kg) could be reduced by 4% approximately. Besides, the Mg^{2+} and Fe^{3+} substitution methods for LZC could effectively reduce the material cost with 318.92 and 308.34 CNY/kg respectively. However, Fe^{3+}-substituted LZC exhibits instability with 4V-class cathodes during charge and discharge. The LZC with Mg^{2+} substitution possesses a relatively high activation energy of 0.40 eV, which cannot operate at a wide range of temperature.

Table S2. Rietveld refinement results from the room-temperature XRD data of the LZC; the space group is $P\bar{3}m1$. The refined lattice parameters are a = 10.9644 Å, b = 10.9644 Å, c = 5.9280 Å.

Atoms	x	y	z	Occ.	site	Sym.	Uiso (Å)
Li1	0.31833	0	0	0.602	6g	2	0.032
Li2	0.33440	0	0.5	0.398	6h	2	0.032
Zr1	0	0	0	0.853	1a	-3m	0.020
Zr2	1/3	2/3	0.53382	0.420	2d	3m	0.020
Zr3	0	0	0.5	0.447	1b	-3m	0.020
Zr4	1/3	2/3	0.95859	0.430	2d	3m	0.020
Cl1	0.10757	-0.10757	0.74605	1	6i	m	0.024
Cl2	0.23006	-0.23006	0.27422	1	6i	m	0.024
Cl3	0.44421	-0.44421	0.72800	1	6i	m	0.024

Table S3. Rietveld refinement results from the room-temperature XRD data of the $LZCa_{0.05}Cl$; the space group is $P\bar{3}m1$. The refined lattice parameters are a = 10.9799 Å, b = 10.9799 Å, c = 5.9388 Å.

Atoms	x	y	z	Occ.	site	Sym.	Uiso (Å)
Li1	0.31352	0	0	0.174	6g	2	0.221
Li2	0.29097	0	0.5	0.877	6h	2	0.221
Zr1	0	0	0	0.388	1a	-3m	0.024
Ca1	0	0	0	0.020	1a	-3m	0.024
Zr2	1/3	2/3	0.51934	0.610	2d	3m	0.024
Ca2	1/3	2/3	0.51934	0.032	2d	3m	0.024
Zr3	0	0	0.5	0.405	1b	-3m	0.024
Ca3	0	0	0.5	0.021	1b	-3m	0.024
Zr4	1/3	2/3	1.01791	0.419	2d	3m	0.024
Ca4	1/3	2/3	1.01791	0.022	2d	3m	0.024
Cl1	0.11195	-0.11195	0.75335	1	6i	m	0.012
Cl2	0.22885	-0.22885	0.22295	1	6i	m	0.012
Cl3	0.44415	-0.44415	0.72618	1	6i	m	0.012

Table S4. Resistances of the ASSBs employed LZC and $LZCa_{0.1}Cl$ with LCO cathode materials fitted by the equivalent electric circuit.

Solid electrolyte	R_{SE} (Ω)	R_{ct1} (Ω)	R_{ct2} (Ω)
LZC	150	45.1	268
$LZCa_{0.1}C$	66.4	8.7	81.7

Table S5. Resistances of the ASSBs employed LZC and $LZCa_{0.1}Cl$ with scNCM811 cathode materials fitted by the equivalent electric circuit.

Solid electrolyte	R_{SE} (Ω)	R_{ct1} (Ω)	R_{ct2} (Ω)
LZC	86.1	50.0	469
$LZCa_{0.1}C$	51.6	14.0	212

References

1 M. R. Busche, D. A. Weber, Y. Schneider, C. Dietrich, S. Wenzel, T. Leichtweiss, D. Schröder, W. Zhang, H. Weigand, D. Walter, S. J. Sedlmaier, D. Houtarde, L. F. Nazar and J. Janek, *Chem. Mater.*, 2016, **28**, 6152-6165.

2 R. Von, *J. Appl. Crystallogr.*, 2014, **47**, 1784-1789.

3 H. Chen and S. Adams, *IUCrJ*, 2017, **4**, 614-625.

4 H. Chen, L. L. Wong and S. Adams, *Acta Crystallogr., Sect. B: Struct. Sci.*, 2019, **75**, 18-33.

5 K. Momma and F. Izumi, *J. Appl. Crystallogr.*, 2011, **44**, 1272-1276.

6 F. Li, X. Cheng, L.-L. Lu, Y.-C. Yin, J.-D. Luo, G. Lu, Y.-F. Meng, H. Mo, T. Tian, J.-T. Yang, W. Wen, Z.-P. Liu, G. Zhang, C. Shang and H.-B. Yao, *Nano Lett.*, 2022, **22**, 2461-2469.

7 Haynes, W.M., D.R. Lide, and T.J. Bruno, CRC Handbook of Chemistry and Physics (97th Edition). 2016-2017: CRC Press.

8 X.-K. Liu, Y.-X. Zhou, F.-H. Mi, X.-L. Ma and C.-W. Sun, *Energy Storage Mater.*, 2024, **72**, 103737.

9 H. Kwak, D. Han, J. Lyoo, J. Park, S. H. Jung, Y. Han, G. Kwon, H. Kim, S.-T. Hong, K.-W. Nam and Y. S. Jung, *Adv. Energy Mater.*, 2021, **11**, 2003190.

10 H. Zhang, Z. Yu, H. Chen, Y. Zhou, X. Huang and B. Tian, *J. Energy Chem.*, 2023, 79, 348-356.